ELSEVIER

J. Non-Newtonian Fluid Mech. 121 (2004) 55–68

Journal of Non-Newtonian Fluid Mechanics

www.elsevier.com/locate/jnnfm

Vortex shedding in cylinder flow of shear-thinning fluids. III Pressure measurements

P.M. Coelho [a], F.T. Pinho [b,*]

[a] *Centro de Estudos de Fenómenos de Transporte, DEMEGI, Faculdade de Engenharia da Universidade do Porto, Rua Dr. Roberto Frias s/n 4200-465 Porto, Portugal*

[b] *Centro de Estudos de Fenómenos de Transporte, DEM, Universidade do Minho, Campus de Azurém, 4800-058 Guimarães, Portugal*

Received 25 December 2003; received in revised form 25 February 2004

Abstract

Measurements of pressure on the cylinder surface for the flow of Newtonian and non-Newtonian fluids around a circular cylinder were carried out, from which several parameters were calculated: the form drag coefficient (C_D), the pressure rise coefficient ($C_{pb} - C_{pm}$) and the wake angle (θ_w). The non-Newtonian fluids were aqueous solutions of CMC and tylose with varying degrees of shear-thinning and elasticity, at weight concentrations of 0.1–0.6% and the experiments encompassed the transition and shear-layer transition regimes. For low Reynolds numbers flows elasticity on the shear layers was responsible for an increase in drag reduction with polymer concentration. Within the shear-layer transition regime the increase of the wake angle and pressure rise coefficient for the more concentrated solutions reduced C_D by narrowing the near wake. For the tylose solutions a good correlation was found between the elasticity number and the mean pressure rise coefficient.

Keywords: Cylinder flow; Viscoelastic; Shear-thinning; Dilute polymeric solutions; Relaxation time; Pressure; Drag; Strouhal number; Laminar; Transition

1. Introduction

The experimental study of the flow of tylose and CMC solutions around cylinders [1,2], is completed here with results from pressure measurements along the cylinder surface. This is part of a wider research programme aimed at investigating cylinder flows of non-Newtonian fluids at large Reynolds numbers and was motivated by both the scarcity of information in the literature and its discrepancy. Next, we review the literature on what concerns pressure measurements since other flow characteristics were reviewed in detail previously [1].

Coelho and Pinho [1] identified and delimited various vortex shedding regimes as a function of the Reynolds and elasticity numbers; in particular the laminar, transition and shear-layer transition regimes. The flow characteristics within each of those flow regimes were then analysed in detail [2], and, in particular, the increase of the Strouhal number and the reduction of, Re^*_{lf} [1] were explained and within the shear-layer transition regime, the formation length and Strouhal number data collapsed onto single curves when plotted against a Reynolds number difference.

In the literature, comparatively very few experiments on external flows of non-Newtonian fluids include pressure measurements. Shah et al. [3] were among the first to experimentally investigate cross flows of non-Newtonian fluids around cylinders (up to Reynolds numbers of about 12,000) and they found that the variation of pressure along the laminar boundary layer was independent of the consistency (k) and power law (n) indices for shear-thinning, elastic, aqueous solutions of CMC.

White [4] observed a reduction in drag and related it with viscoelastic effects especially with non-negligible normal stress differences. The drag reduction seen in flows of polyethylene oxide (PEO) was consistent with visualizations made by other authors with PEO solutions, who observed a delay in the boundary layer separation and a narrow wake.

* Corresponding author.
E-mail addresses: pmc@fe.up.pt (P.M. Coelho), fpinho@dem.uminho.pt, fpinho@fe.up.pt (F.T. Pinho).

[1] Re^*_{lf} is the critical Reynolds number marking the sudden decrease of the formation length.

0377-0257/$ – see front matter © 2004 Elsevier B.V. All rights reserved.
doi:10.1016/j.jnnfm.2004.04.004

Nomenclature

C_D	drag coefficient
C_p	pressure coefficient
C_{pb}	base pressure coefficient
C_{pm}	minimum pressure coefficient
$C_{pb} - C_{pm}$	pressure rise coefficient
D	cylinder diameter (m)
l_f	formation length (m)
l_{fc}	critical formation length, corresponds to the value of l_f just prior to its sudden drop (m)
$Lu(x)$	longitudinal turbulence length scale base on u (m)
n	power law index
Re	Reynolds number, $Re \equiv \rho\, U_\infty\, D/\eta_{ch}$
$\overline{u'}$	average value of the rms of the instantaneous longitudinal velocity
U_∞	free-stream velocity (m/s)
We	Weissenberg number, $We \equiv \lambda_e U_\infty / D$

Greek letters

η	dynamic viscosity (Pa s)
$\dot{\gamma}$	shear rate (s^{-1})
λ_e	relaxation time (s)
ρ	fluid density (kg/m^3)
θ	angle measured from the forward stagnation point, see inset in Fig. 2
θ_W	wake angle, $\theta_W = (\theta_{W,1} + \theta_{W,2})/2$

Subscripts

bbp	end of the region where the power spectra distribution shows a broad basis at peak frequency
ch	characteristic parameter
etr	the end of transition regime
lf	sudden drop in formation length
otr	onset of transition regime
w	wall
1	refers to angle comprised between 0 and π
2	refers to angle comprised between π and 2π
75	75° from forward stagnation point

Superscripts

$'$	refers to Reynolds number with η_{ch} at $\dot{\gamma}_{ch} \equiv \dot{\gamma}_{w,75°}$
*	refers to Reynolds number with η_{ch} at $\dot{\gamma}_{ch} \equiv U_\infty/(2D)$

Symbols used in figures

×	water
+	glycerine and water mixture
●	0.4% CMC
◆	0.2% CMC
○	0.6% tylose
△	0.4% tylose
◇	0.3% tylose
□	0.2% tylose

According to Hoyt and Sellin [5] another early work on drag in non-Newtonian cylinder flows was that of McClanahan and Ridgely (1968). They found a drag increase for $10^4 < Re < 4 \times 10^4$ at low polymer concentrations and drag reduction at higher polymer concentrations. The measurements of hydrodynamic and heat transfer characteristics of elastic fluids with constant shear viscosity, Boger fluids, by James and Acosta [6] and James and Gupta [7] were limited to lower maximum Reynolds numbers of 50 and 200, respectively, and cylinder diameters lower than 0.36 mm corresponding to large aspect ratios (higher than 160). Above a critical Reynolds number, the drag coefficient and Nusselt number were found to depend only on the Weissenberg number.

A fairly detailed investigation with Boger fluids, was also carried out by Sarpkaya et al. [8] who measured the surface pressure distribution, drag force, vortex shedding frequency, angle of separation and some effects of free-stream turbulence. The presence of additives was found to advance flow characteristics normally observed at higher Reynolds numbers and to increase the cylinder base pressure thus decreasing the drag coefficient. Their Reynolds numbers were rather restricted ($5 \times 10^4 < Re < 3 \times 10^5$), but much higher than in previous works.

Using a semicircular cylinder with the round side facing the approach stream, Kiya et al. [9] injected polyethylene oxide and polyacrylamide (PAM) in the boundary layer, at a Reynolds number of 2×10^5. The base pressure increased with polymer concentration until a saturation effect took place and their explanation for this increase is quoted: "Since the aqueous solutions of PEO and PAM exhibit the viscoelastic property, the shear layers shed from the cylinder, which include the polymer solutions, will diminish the interactions between fluid inside and outside the base region. This will lead to an increase in the base pressure." Similar conclusions were reached by Cadot and Lebey [10] and Coelho and Pinho [2] to explain the increase in formation length in the flow of non-Newtonian fluids around circular cylinders.

Kato and Mizuno [11] measured the total drag in non-Newtonian cylinder flows for Reynolds numbers up to 5×10^4. Their cylinder diameters ranged from 4 to 26 mm and the aspect ratio varied from 1 to 500. For 0.2–0.5% PEO solutions and $Re < 100$ the drag coefficient was found to be only a function of the Reynolds number and was independent of the elasticity and the power law index. For the more dilute PEO solutions, from 30 to 300 ppm, the Reynolds number ranged from 10^3 to 5×10^4 and drag

reductions of up to 33% were measured for the more concentrated solutions. For 30 ppm PEO and pure water the pressure distributions around the cylinder were found to be identical, but for the 50 ppm PEO solution the base pressure rose 30% and the boundary layer separation was delayed by approximately 10°. The main reason why James and Gupta [7] have detected an increase in drag coefficient, contrary to the results of Kato and Mizuno [11], lies in the fact that the former used very small cylinder diameters, 0.15–0.36 mm. According to Metzner and Astarita [12], very small cylinder diameters lead to high Deborah numbers which imply a solid-like material response in the boundary layer. This leads to a free-stream velocity independent behaviour and an increase in C_D.

These works, which represent most of the published literature on drag with polymer solutions, were carried out with elastic, weakly shear-thinning fluids and investigated the effects of rheology on the drag coefficient. In contrast, moderately shear-thinning fluids are used here to investigate effects of rheology on various quantities: the drag coefficient, the wake angle and the pressure rise coefficient. Besides, this work continues our previous investigations [1,2], where the various shedding flow regimes were identified and partially characterized.

Flow characteristics depend not only on fluid rheology, but in a strong manner on geometric issues such as the aspect ratio and the existence of end plates, as well as on free-stream turbulence. All these differ in all past works, as well as in this work, therefore attempting to relate the various research conclusions is often a very difficult task, touching on the impossible.

In the next section, the experimental facility and the main fluid characteristics are briefly described; more details are presented in [1]. In Section 3, the dimensionless parameters that will be used in the data reduction analysis are summarised and the variables that have more effect on the cylinder drag coefficient (C_D) are briefly review. Then, in Section 4 the new results are presented and discussed after a brief summary of the flow identification is carried out [1].

2. Experimental facility and fluid characteristics

The flow measurements were carried out in a water tunnel having a 6:1 contraction before a transparent test section of 197 mm height and 120 mm width. Only one cylinder was used in the pressure experiments: it had a diameter of 19.7 mm, leading to a blockage ratio of 10% and an aspect ratio, L/D, of 6:1.

A diode fibre-optic laser-Doppler system from INVENT, model DFLDA, was used to characterize the free stream. This system was described in detail by Coelho and Pinho [1].

The pressure measurements were carried out with three different P305D Validyne differential pressure transducers, with different full scale values of 80, 200 and 880 mm H_2O respectively.

One pressure tap of 0.3 mm diameter was drilled on the surface of the cylinder which was rotated with 5° increments to allow measurement of the full pressure profile relative to the static pressure measured at the test section wall. The small size of the pressure tap meant that for the more viscous fluids (0.4% CMC and 0.6% tylose), the response time was slow, of about two minutes, in spite of the fact that the connecting tubes were filled with water.

The pressure transducers were connected to a 386 PC via a data acquisition Metrabyte board DAS8 and a Metrabyte ISO4 multiplexer board. For each angular location a sample of 2000 readings was taken and the statistical quantities were calculated by purpose-built software, with an estimated overall uncertainty of 4.3, 0.8 and 1.2% for the three pressure transducers. Based on the literature [13,14], the measured pressure differences and rheological information for similar fluids from [15], the hole pressure error was estimated not to exceed 2% in the worst case (0.4% CMC solution at the highest Reynolds number).

High and low molecular weight polymers were dissolved in water to produce elastic and weakly elastic shear-thinning fluids, respectively, and the results compared to those of two Newtonian fluids of different viscosities. The weakly elastic fluids were aqueous solutions of 0.2, 0.3, 0.4 and 0.6% by weight concentration of a methyl hydroxyethyl cellulose, brand name tylose, grade MH 10,000 K from Hoechst, with a molecular weight of 6000 kg/kmol. The more elastic fluids were aqueous solutions of carboxymethyl cellulose sodium salt (CMC), grade 7H4C from Hercules, with a molecular weight of 300,000 kg/kmol, at weight concentrations of 0.2 and 0.4%. To prevent bacteriological growth and degradation 0.02% w/w of a biocide, Kathon LXE 1.5% from Rohm & Haas, was added to all solutions of CMC. Only two solutions of CMC were used, because the CMC solutions degraded much faster than the tylose solutions and the pressure measurements were relatively long. The Newtonian fluid was a mixture of w/w 40% water and 60% glycerine, having a viscosity of 0.0073 Pa s at 25 °C, the temperature at which all tests were carried out. The viscosity and other rheological properties of these non-Newtonian fluids are presented in detail elsewhere [1], but here they are briefly summarized.

All the solutions exhibited shear-thinning behaviour, as can be seen in the viscosity–shear rate plot of Fig. 1, with the CMC solutions being more shear-thinning than the tylose solutions at equal polymer concentrations. The Carreau–Yasuda viscosity model (Eq. (1)) was fitted to the data (full lines in Fig. 1) and their parameters are listed in Table 1.

$$\mu = \mu_\infty + (\mu_0 - \mu_\infty)\left[1 + (\lambda\dot{\gamma})^a\right]^{n-1/a} \quad (1)$$

The elasticity of the solutions was assessed from creep and oscillatory shear flows. With the creep test a relaxation time (λ_e) was determined for some of the solutions and they are listed in Table 2 along with the corresponding precision (random) uncertainty at a 95% confidence level. Here the relaxation time is determined as the ratio between the shear

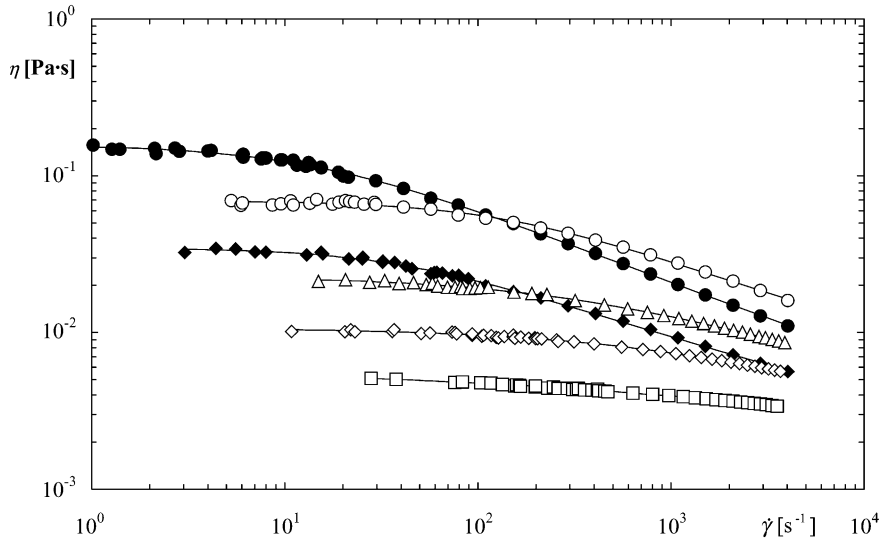

Fig. 1. Viscosity vs. shear rate at 25 °C. Full line: adjusted Carreau–Yasuda viscosity model. Symbols as in notation.

Table 1
Parameters of the Carreau–Yasuda viscosity model for tylose and CMC solutions

Solution	η_0 (Pa s)	η_∞ (Pa s)	λ (s)	a	n	$\dot{\gamma}$ (s^{-1})
0.4% CMC	0.1598	0.0008	0.0681	0.991	0.513	1–4000
0.2% CMC	0.0358	0.0008	0.0271	1.043	0.581	30–4000
0.6% tylose	0.0705	0.0008	0.00720	1.006	0.558	5–4000
0.4% tylose	0.0227	0.0010	0.00304	0.741	0.608	10–4000
0.3% tylose	0.0107	0.0010	0.00095	0.653	0.594	10–4000
0.2% tylose	0.00614	0.0008	0.00011	0.290	0.631	20–4000

Table 2
Relaxation time of some solutions from creep tests at 25 °C and corresponding uncertainty

	0.4% CMC	0.2% CMC	0.6% tylose	0.4% tylose	0.3% tylose	0.2% tylose
λ_e (s)	0.488	0.162	0.389	0.053	0.0212	0.0165
$\Delta\lambda_e/\lambda_e$	±6%	±14%	±3%	±19%	–	–

deformation, γ_0, and the shear rate, $\dot{\gamma}_\infty$, at a limiting zero shear stress ($\lambda_e \equiv \lim_{\tau\to 0}(\gamma_0/\dot{\gamma}_\infty)$), following the procedure outlined in Bird et al. [16]. The numerical values of λ_e for the 0.3% and 0.2% tylose solutions were estimated according to a procedure outlined by Coelho and Pinho [1] and are also given in Table 2.

3. Pressure coefficient, related quantities and other effects

The pressure distribution around a cylinder is characterized by various quantities introduced in this section. A discussion of the flow properties affecting the pressure distribution is also presented.

Profiles of dimensionless pressure around a cylinder, in the form of the pressure coefficient C_p of Eq. (2), is shown in Fig. 2 for the 0.2% CMC solution at a Reynolds number Re^* of 565 and for the glycerine–water mixture at $Re = 863$. The viscosity used to calculate Re^* is based on a characteristic shear rate of $U_\infty/(2D)$, for reasons explained in detail by Coelho and Pinho [1]. The pressure coefficient is defined as:

$$C_p \equiv \frac{P - P_\infty}{\rho U_\infty^2/2}, \tag{2}$$

where P, P_∞, ρ and U_∞ stand for the pressure on the cylinder surface, the free-stream static pressure, fluid density and free-stream velocity, respectively.

C_p is equal to 1 in the forward stagnation point, then it decreases to the minimum pressure coefficient, C_{pm}, somewhere at an angle θ of about 70–73° measured from the forward stagnation point. With increasing θ, C_p rises again to a constant value at the back of the cylinder called the base pressure coefficient, C_{pb}. Its symmetric value, $-C_{pb}$, is called the suction coefficient. The free-stream static pressure, P_∞, was calculated from the stagnation pressure,

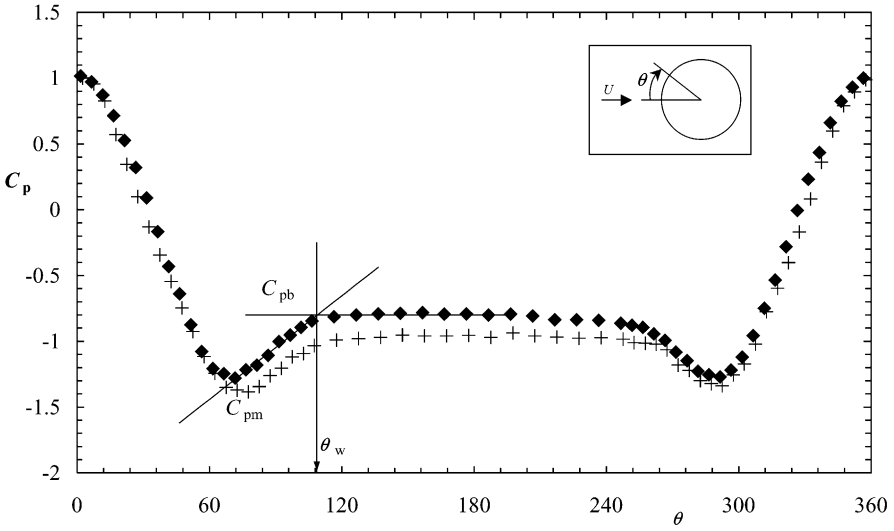

Fig. 2. Mean pressure distribution, C_p, around the cylinder for the solution of 0.2% CMC at $Re^* = 565$, and the glycerine–water mixture at $Re = 863$.

measured at the cylinder forward stagnation point, and the measured free-stream velocity.

Slight asymmetries in the mean pressure distribution were detected at angles θ ranging from 70° (290°) to 100° (260°), but never exceeding 7 and 3% for the tylose and CMC solutions, respectively.

The mean pressure distributions were processed to evaluate various quantities: the form drag coefficient, C_D, was obtained by integration of the pressure profile as in Eq. (3) and the base pressure coefficient, C_{pb}, was defined as the average C_p in the wake region, see Eq. (4).

$$C_D = \frac{\int_0^{2\pi} \cos\theta \cdot P \cdot d\theta}{\rho U_\infty^2}, \tag{3}$$

$$C_{pb} = \frac{\int_{\theta_{w,1}}^{\theta_{w,2}} (P - P_\infty)/(\rho U_\infty^2/2) \cdot d\theta}{\theta_{w,2} - \theta_{w,1}} = \frac{\int_{\theta_{w,1}}^{\theta_{w,2}} C_p \cdot d\theta}{\theta_{w,2} - \theta_{w,1}}. \tag{4}$$

Other relevant quantities are the minimum pressure coefficient, C_{pm}, and an estimate of the separation angle of the boundary layer also known as wake angle, θ_w. θ_w was determined and defined as suggested by Niemann, following Güven et al. [17]: the angle corresponding to the interception of an horizontal line, representing the base pressure coefficient, with the slopping straight line fitted to the C_p values in the adverse pressure gradient region (see sloping line in Fig. 2). The two values of wake angle, $\theta_{W,1}$ and $\theta_{W,2}$, were averaged to determine θ_W, as was the case for the two minimum pressure coefficients, $C_{pm,1}$ and $C_{pm,2}$.

Fig. 2 is representative of pressure distributions on the cylinder surface in that profiles collapse within the ±60° cylinder forward region, and show the effects of Reynolds number and fluid rheology elsewhere.

The pressure rise coefficient, $C_{pb} - C_{pm}$, which is a measure of the pressure rise sustained by the boundary layer prior to separation [18], was also calculated. This coefficient and the various quantities just defined are affected by the Reynolds number, the free-stream turbulence, blockage ratio, aspect ratio and the presence of end plates as discussed next.

According to Surry [19], who studied the effects of free-stream turbulence on subcritical Newtonian cylinder flows (at a Reynolds number of 40,000), a decrease in the Taylor parameter can increase the drag coefficient. The Taylor parameter, T, is given by:

$$T = \frac{\overline{u'}}{U_\infty} \left(\frac{D}{Lu(x)} \right)^{1/5}, \tag{5}$$

where $\overline{u'}$, D and $Lu(x)$ stand for the average value of the rms of the instantaneous longitudinal velocity, cylinder diameter and longitudinal turbulence length scale based on the longitudinal component of the velocity. The free-stream turbulence in this work varied between 6 and 3%, as presented in detail by Coelho and Pinho [1]. Other works in the literature have values of turbulence intensity of the order of 2% or less at values of Reynolds number similar to ours.

The effect of blockage on the drag coefficient has been more thoroughly investigated [18,20–22]. For a 10% blockage and $Re > 10^4$, West and Apelt [22] showed that any of the drag coefficient correction methods presented in their work resulted in poorer values than the original uncorrected data. Hence, considering also the unknown effects of non-Newtonian rheology on blockage, it was decided not to apply any corrections to the present data.

West and Apelt [22] also studied the effect of aspect ratio on the drag coefficient and observed an increase in C_D with a decrease in the aspect ratio, for $Re > 10^4$. For $Re \in [200, 2 \times 10^4]$ Norberg [23] investigated the influence of the aspect ratio on the suction coefficient, which has a similar behaviour to that of C_D. At high Reynolds numbers he noticed the

same pattern as that reported by West and Apelt [22], i.e. an increase in suction coefficient with a decrease in the aspect ratio, but for $Re < 8 \times 10^3$ the opposite was found.

From these findings and given the different flow conditions of our experiments and those in the literature, different values of L/D, blockage ratio and free-stream turbulence, the meaningful comparisons are those between Newtonian and non-Newtonian fluids under similar flow conditions, i.e. with similar levels of free-stream turbulence and with the same geometry. Therefore, the data from the glycerine–water mixture obtained in this work will be used henceforth as a reference for comparisons with the data for non-Newtonian fluids.

4. Results and discussion

Three flow regimes were clearly identified and delimited for each fluid by Coelho and Pinho [1]: the laminar vortex shedding regime; the transition regime, which includes the A- and B-modes of shedding; and the shear-layer transition regime, where the laminar-turbulent transition takes place in the shear layers. Table 3 summarises these findings by listing the various critical Reynolds numbers and their uncertainties for the 20 mm cylinder diameter. Re^*_{otr} and Re^*_{etr} represent the onset and end of the transition regime, Re^*_{lf} marks the sudden drop in formation length and consequently indicates the onset of the shear-layer transition regime whenever $Re^*_{lf} > Re^*_{etr}$. The corresponding value of l_f/D is listed in the same column. Finally, Re^*_{bbp} designates the end of the region where the power spectrum distribution shows a broad basis at peak frequency.

Next, the variations of drag coefficient, pressure rise coefficient and wake angle with Reynolds number are presented and the relationships between those parameters and the critical Reynolds numbers are sought. A more detailed analysis is carried out later for data pertaining to the shear-layer transition regime and, at the end, the variations in the pressure rise coefficient are tentatively related with fluid elasticity.

4.1. Form drag coefficient

The C_D variation with the Reynolds number is presented in Fig. 3 for all fluids. The full line represents the Wieselsberger data for Newtonian fluids, taken from Roshko [20], under quasi-ideal conditions of low free-stream turbulence, low blockage ratio and high aspect ratio.

As is know from the literature [11,22,23] for $Re > 2 \times 10^4$ there is an increase of C_D as blockage ratio increases and the aspect ratio decreases, and this also occurs in our

Table 3
Critical Reynolds numbers marking the onset or the end of flow regimes (20 mm cylinder). From Coelho and Pinho [1]

Fluid	Re^*_{otr}	Re^*_{etr}	Re^*_{lf}; l_f/D	Re^*_{bbp}
0.4% CMC	165 (±9.0%)	316 (±12.1%)	275 (±7.0%); 4.4	416 (±26.4%)
0.2% CMC	178 (±8.9%)	525 (±9.2%)	356 (±6.3%); 4.5	1160 (±10.4%)
0.6% tylose	Not detected	Not detected	175 (±3.7%); 3.8	415 (±11.9%)
0.4% tylose	143 (±13.3%)	555 (±9.9%)	1090 (±2.5%); 2.7	1490 (±11.3%)
0.3% tylose	Hard to detect	1160 (±11.5%)	1850 (±3.9%); 2.9	2370 (±8.8%)
0.2% tylose	Hard to detect	2060 (±9.6%)	1950 (±8.3%); 2.3	4100 (±12.4%)
Glycerin + water	717 (±12.5%)	1890 (±11.8%)	2000 (±7.1%); 3.4	5270 (±10.6%)

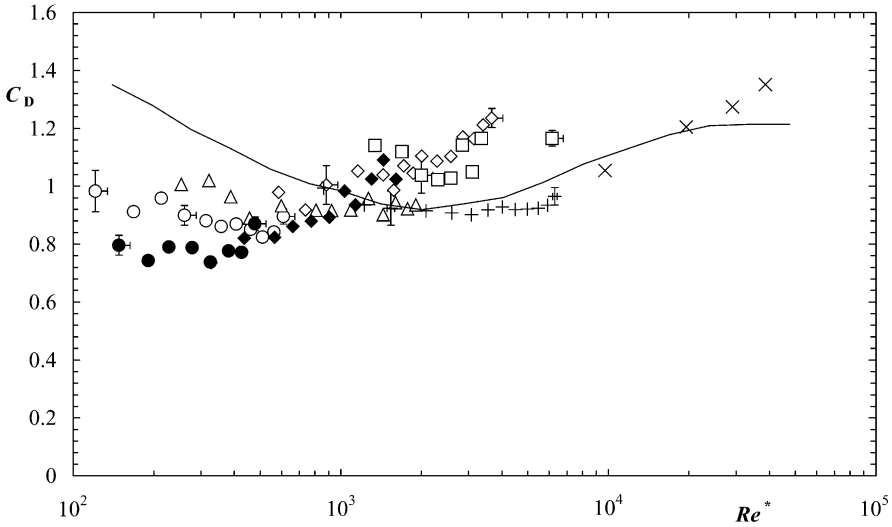

Fig. 3. Variation of form drag, C_D, with Re^*. Symbols as in notation, full line: Wieselsberger [20]; (I, ⊢) uncertainties in the values of C_D and Re^*.

facility. At low Reynolds numbers ($20 < Re < 10^4$) Kato and Mizuno [11] and Norberg [23] noticed a reduction of C_D when L/D decreased. The opposing effects of blockage and aspect ratios at low Reynolds numbers tend to cancel since the experimental data follow the line of Wieselsberger pertaining to low blockage and high aspect ratio.

For Reynolds numbers below 800 there is a reduction of the drag coefficient relative to the Newtonian values, and this is quite clear in the lower C_D values for the more concentrated polymer solutions, a finding also made by Kato and Mizuno [11]. The main reason for this difference in C_D is fluid elasticity. As shown in references [2,10], elasticity reduces the turbulent shear stress in the shear layer, but it can also reduce the effect of Kelvin–Helmoltz instabilities, which are present for $Re > 180$, according to Persillon and Braza [24] and Prasad and Williamson [29]. Generally speaking, the interaction between the shear layer and the recirculating bubble decreases with elasticity, consequently the entrainment of fluid from the formation region is reduced, and the formation length increases. To maintain the equilibrium of forces within the recirculating bubble the base pressure has to increase in order to compensate for the lower shear stresses, thus reducing the drag coefficient. More details about the balance of forces acting within the recirculating bubble are explained by Balachandar et al. [25]. For a semicircular cylinder Kiya et al. [9] have also observed that a reduction of the interaction between the free shear layers and the recirculating bubble decreased the drag coefficient. Larger reductions of C_D by fluid elasticity than by shear-thinning was also observed for the flow around a sphere by Acharya et al. [26,27].

For Reynolds numbers above 800 the analysis of Fig. 3, is complicated by differences in flow regime (see Table 3): the critical Reynolds number for the beginning of the shear-layer transition regime, usually Re^*_{lf}, is not the same for all solutions and is a strong function of fluid elasticity [2]. As is known from [28,29] this flow regime has a significant impact on the drag coefficient; basically, C_D increases when the laminar-turbulent transition takes place in the free shear layers and moves upstream towards the cylinder. The variation of C_D for high Reynolds number flows is analysed in Section 4.4, where a more detailed study of the shear-layer transition regime is presented.

Fig. 4 shows the relationship between the drag coefficient, the formation length, l_f, and the critical Reynolds numbers in Table 3. Generally speaking, the drag coefficient starts to increase in the vicinity of the Reynolds number where there is a sudden decrease in the formation length, Re^*_{lf}, in agreement with findings from [28,29]. The variation of formation length is opposite to that of the drag coefficient as explained by Bearman[2]. Apart from that, there is no apparent relation between the other critical Reynolds numbers and the variations of C_D.

[2] According to Woo et al. [30].

4.2. Pressure rise coefficient, $C_{pb} - C_{pm}$

In this section the variation of the pressure rise coefficient with the Reynolds number is analysed. According to [17,18], the blockage and the aspect ratio do not significantly affect this coefficient in the supercritical and transcritical regimes.

Fig. 5 shows the variation of $C_{pb} - C_{pm}$ with Reynolds number for all the solutions used. The pressure rise coefficient decreases with Reynolds number, but the variation is not very intense. For the tylose solutions there is a clear increase in $C_{pb} - C_{pm}$ with the polymer concentration, which is not observed for the CMC solutions.

For a better insight onto the relationship between these various quantities, the same $C_{pb} - C_{pm}$ data were plotted for each fluid individually, together with data on the critical Reynolds numbers and formation length, but no significant influence was found.

4.3. Wake angle, θ_w

The variation of wake angle with Reynolds number Re^* is represented in Fig. 6 for all fluids. The full lines delimit the range of values that can be found in the literature, as compiled by Son and Hanratty [31], and pertains to Newtonian fluids. All the data lie on the lower limit of this range but, according to Güven et al. [17], the wake angle is an estimate of the true boundary layer separation angle which takes on lower values than the real separation angle, at least in the supercritical and transcritical regimes. The same occurs at these low Reynolds numbers where the wake angle, θ_w, can still be considered a fairly good estimate of the separation angle.

As with the pressure rise coefficient, the wake angle data were reproduced individually to investigate possible relations with the critical Reynolds numbers and formation length, but no visible correlations were found. However, there is a common characteristic to all solutions in that as the formation length decreases with the Reynolds number the same happens with the wake angle, i.e. the boundary layer separation point moves upstream on the cylinder surface as l_f decreases.

4.4. The shear-layer transition regime

Woo et al. [30] quoted Bearman's finding that there is a good correlation between the formation length and the pressure base coefficient. Since the variations of C_{pb} and C_D are opposite, C_D is represented as a function of D/l_f in Fig. 7 for the data pertaining to the shear-layer transition regime; the plot shows a good correlation between the two quantities. This is also in agreement with another of Bearman's findings quoted in [30]: that there is an increase in C_D with a decrease in l_f.

To assist in analysing data, Fig. 8 plots the ratio l_f/l_{fc} as a function of $Re^* - Re^*_{lf}$ (these data were taken from [2]). The critical formation length l_{fc} corresponds to the

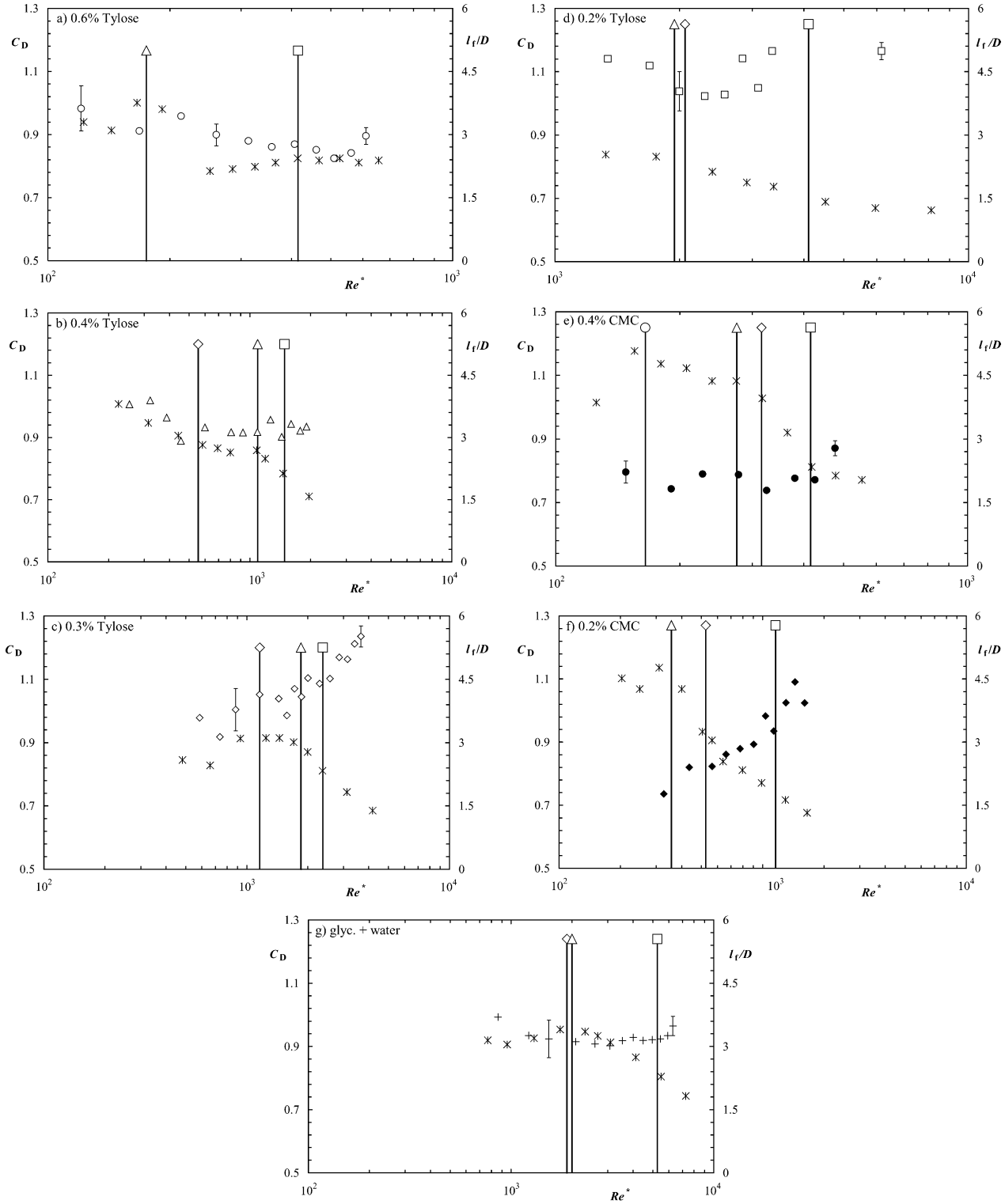

Fig. 4. Comparison between the form drag, C_D, and the critical Reynolds numbers and formation length, l_f/D taken from [1]. Symbols as in notation for C_D; (⊠) l_f/D; vertical lines: (○) Re^*_{otr}, (◇) Re^*_{etr}, (△) Re^*_{lf}, (□) Re^*_{bbp}. (⊥) Uncertainties in the values of C_D.

value of l_f just prior to its sudden drop, at $Re^* = Re^*_{lf}$. The more elastic solutions of CMC and 0.6% tylose show the highest relative reduction in the formation length, whereas the smallest variations are those of the Newtonian fluid. As discussed by Coelho and Pinho [2], these observations are consistent with and extend the findings of Cadot and Kumar [32] that fluid elasticity stabilise the shear layers. In fact, as the shear layers become turbulent it is expected

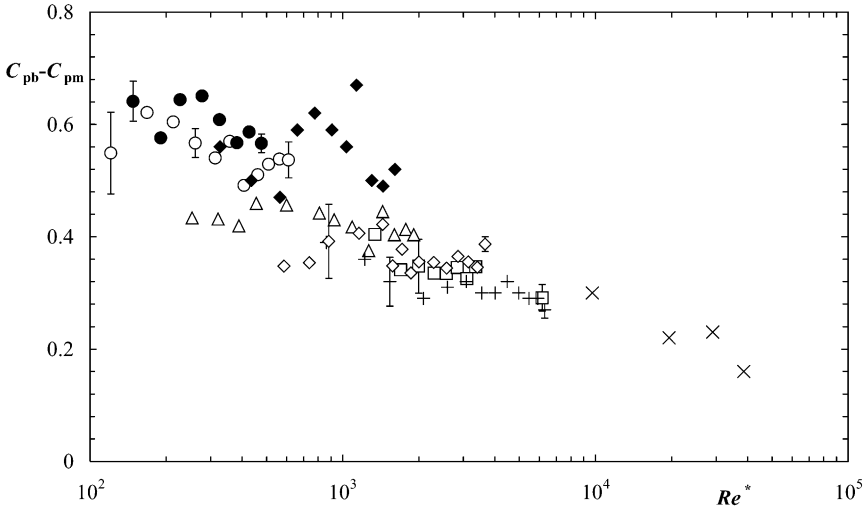

Fig. 5. Variation of the pressure rise coefficient, $C_{pb} - C_{pm}$, with Re^*. Symbols as in notation. (I) Uncertainties in the values of $C_{pb} - C_{pm}$.

that those that are more stable will be more extensively modified.

In Fig. 8, the behaviour of the 0.6% tylose solution is completely different from that of the others fluids. This fluid was the only solution for which the transition regime was suppressed [1] and arguably delayed the upstream progress of the shear-layer transition. Such a delay impairs the progressive decrease in formation length so typical of this flow regime and leads to higher Strouhal numbers [2], because the shear layers are thinner, in this way promoting vortex shedding.

Since the critical Reynolds number for the onset of the shear-layer transition regime (Re^*_{lf}) is not the same for all solutions [1], significant differences in C_D, $C_{pb} - C_{pm}$ and θ_w are artificially induced in the data comparison by the fact that the shear layers for different fluids are at different stages of development at identical Reynolds numbers. These differences can therefore be removed by plotting the data as a function of $Re^* - Re^*_{lf}$ as suggested by Coelho and Pinho [2]. This abscissa will also emphasise elastic effects because, in principle, at the same $Re^* - Re^*_{lf}$ the shear layers should be similar unless rheological characteristics, other than viscous effects, are important. The data on C_D, $C_{pb} - C_{pm}$ and θ_w are then presented as a function of $Re^* - Re^*_{lf}$ in Figs. 9–11 respectively.

The similarity between the relative positions of the C_D curves in Figs. 7 and 9 is not totally unexpected given the good collapse of all the formation length curves when represented against $Re^* - Re^*_{lf}$ (see Fig. 12 in [2]).

Generally speaking, the intense reduction of l_f/l_{fc} with polymer concentration seen in Fig. 8 does not lead to an increase in drag coefficient; quite the opposite, fluids exhibiting the strongest reduction of l_f/l_{fc} have the lowest values of the drag coefficient seen in Fig. 9, with the exception of the

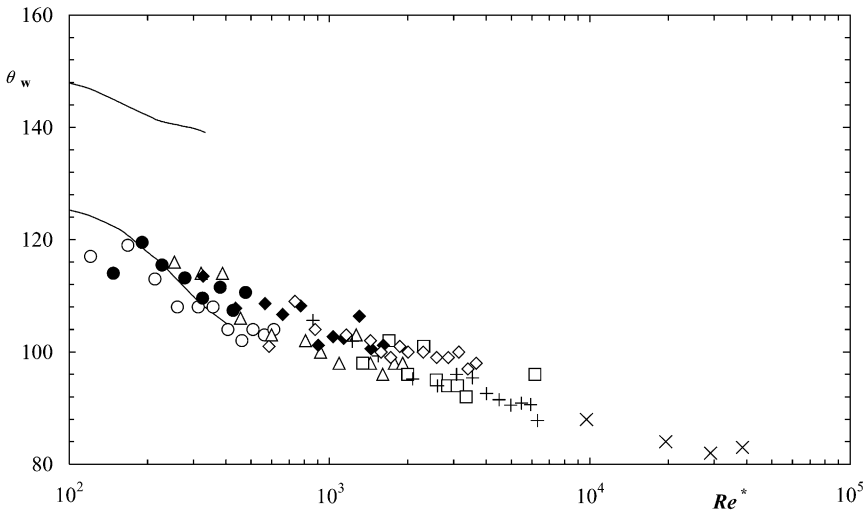

Fig. 6. Variation of the wake angle, θ_w, with Re^*. Symbols as in notation. Full lines, Son and Hanratty [31].

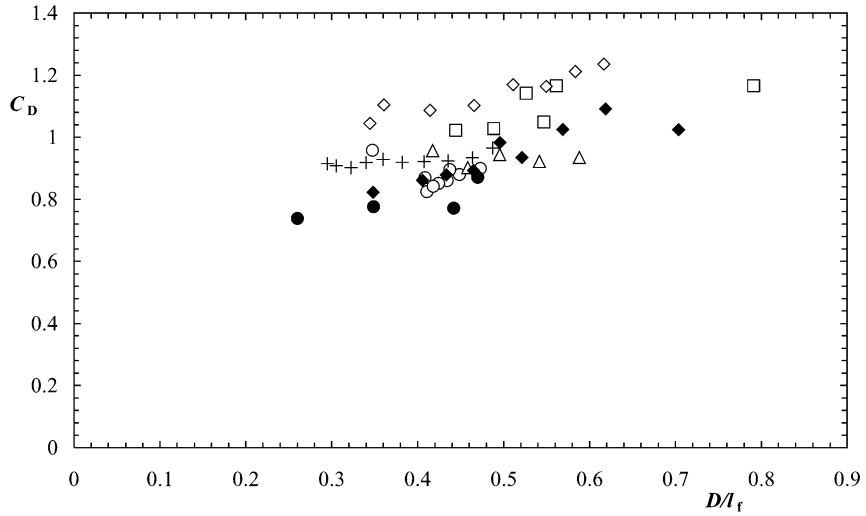

Fig. 7. Variation of form drag, C_D, with the inverse of the formation length, D/l_f, in the shear-layer transition regime. Symbols as in notation.

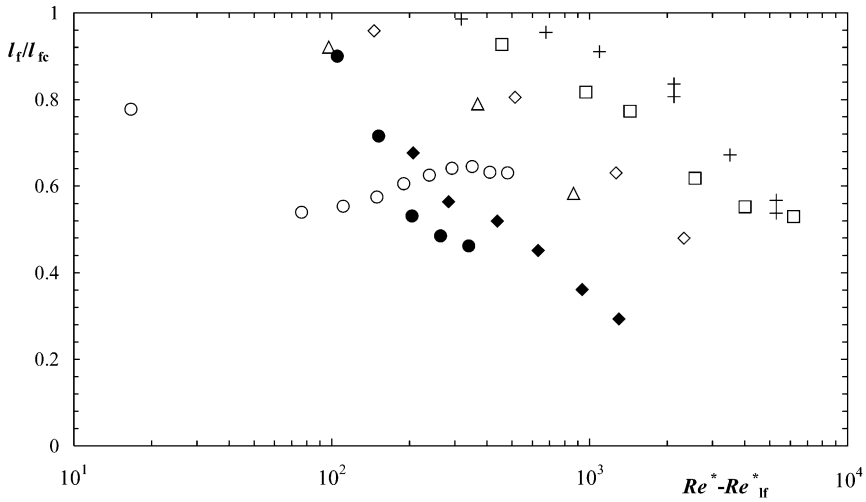

Fig. 8. Ratio of formation length l_f/l_{fc} as a function of $Re^* - Re^*_{lf}$ in the shear-layer transition regime. Symbols as in notation.

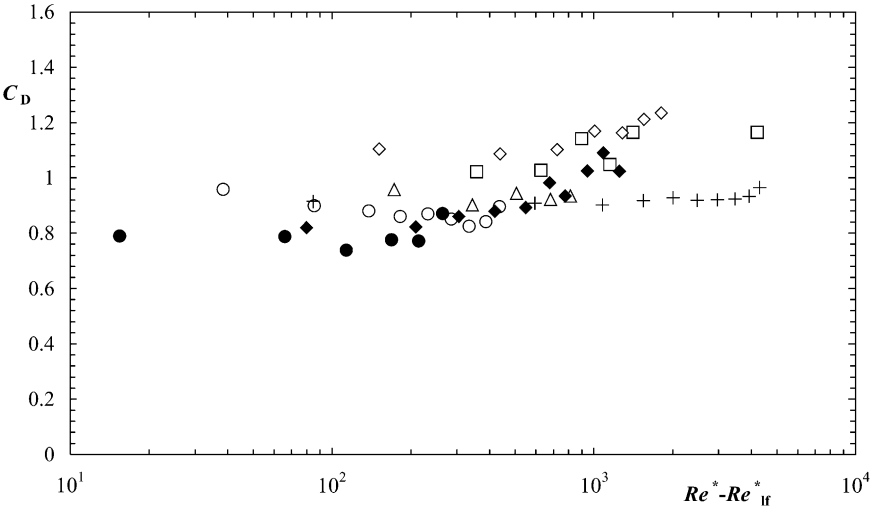

Fig. 9. Variation of form drag, C_D, with $Re^* - Re^*_{lf}$ in the shear-layer transition regime. Symbols as in notation.

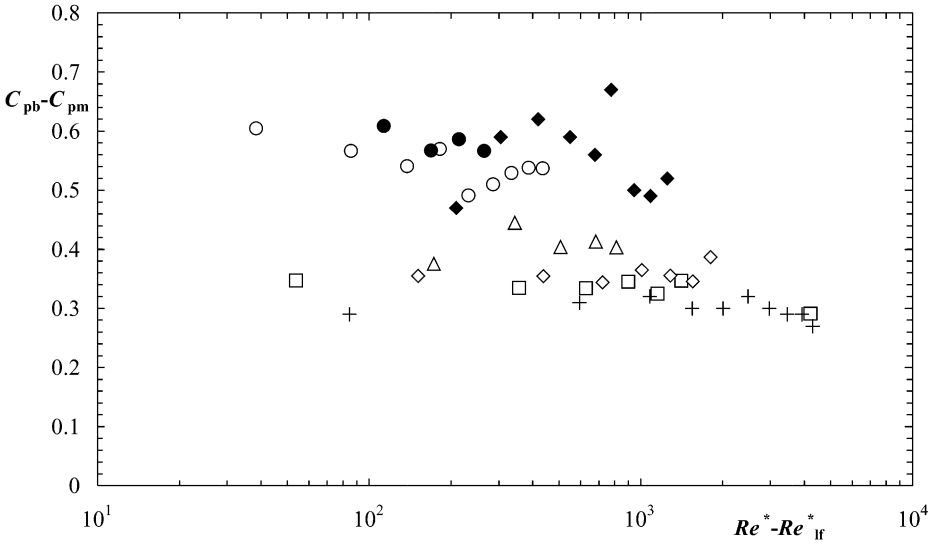

Fig. 10. Variation of the pressure rise coefficient, $C_{pb} - C_{pm}$, with $Re^* - Re^*_{lf}$ in the shear-layer transition regime. Symbols as in notation.

Newtonian fluids. This is due to the simultaneous increase of the pressure rise coefficient and wake angle with polymer concentration (cf. Figs. 10 and 11), both of which concur to reduce C_D by narrowing the wake.

Analysing the behaviour of the CMC solutions in Figs. 7–11, we do not see any remarkable differences with polymer concentration. A homogenisation of the Strouhal number behaviour was also detected for these same solutions by Coelho and Pinho [2] and this was related to particular end effects seen with these fluids. Although the CMC solutions exhibit the lowest values of l_f/l_{fc}, they also have the highest pressure rise coefficient and wake angle; these two quantities determine the lowest drag coefficients because the wake is very narrow.

The tylose solutions show an initial increase in C_D, when the polymer concentration raises from 0% (Newtonian) to 0.2% and then to 0.3% (cf. Figs. 7 and 9). This is consistent with the l_f/l_{fc} reduction in Fig. 8, and with the corresponding low values of $C_{pb} - C_{pm}$ and θ_w, in Figs. 10 and 11, respectively. The increase in turbulent shear-layer stress, responsible for the reduction of formation length, increases the drag coefficient [25,29].

When the tylose concentration goes from 0.3 to 0.4% and then to 0.6%, C_D is reduced and this is consistent with the higher values of the pressure rise coefficient and wake angle. So, it seems that the ability of the boundary layer to sustain a higher pressure rise prior to separation (higher values of $C_{pb} - C_{pm}$), thus reducing the drag coefficient by narrowing the wake, more than compensates the opposite effect on C_D of the transition taking place in the free shear layers.

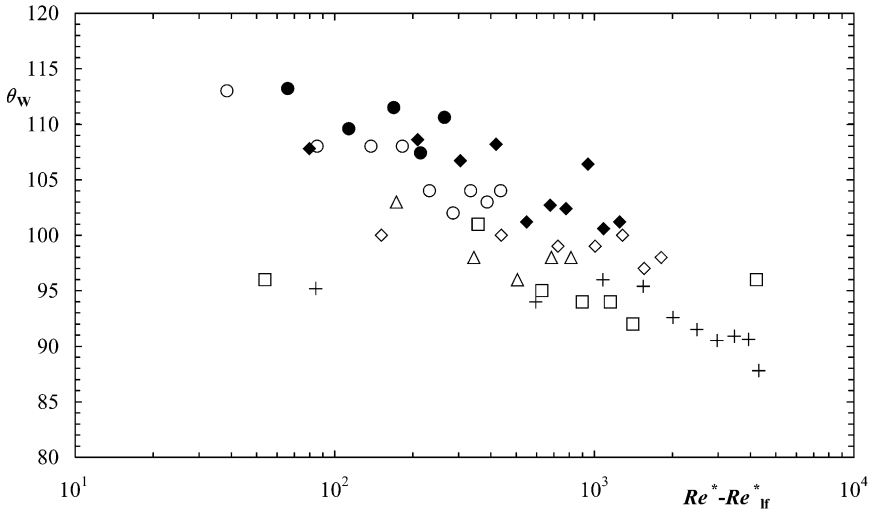

Fig. 11. Variation of the wake angle, θ_w, with $Re^* - Re^*_{lf}$ in the shear-layer transition regime. Symbols as in notation.

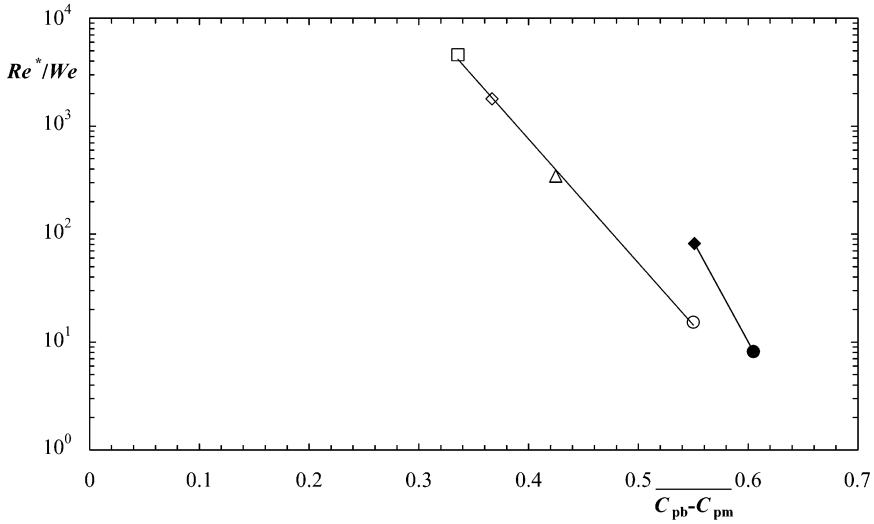

Fig. 12. Variation of elastic number Re^*/We with the average pressure rise coefficient, $\overline{C_{pb} - C_{pm}}$ Symbols as in notation.

4.5. Pressure rise coefficient and elasticity

It is evident in Fig. 10 that the pressure rise coefficient grows with polymer concentration. In the region comprised by the minimum and base pressure coefficients (C_{pm} and C_{pb}, respectively cf. Fig. 2) the polymer molecules are subjected to compression and it is known that elastic fluids exhibit greater resistance to normal deformations than inelastic fluids [16]. This is translated as higher extensional viscosities. In adverse pressure gradient regions the longitudinal velocity gradient du/dx is negative, i.e. since normal strains are resisted more intensively by elastic fluids there is consequently a retardation of the velocity profile and in particular of the boundary layer separation point which moves downstream. In this way, upstream of the boundary layer separation point, the elastic fluids are able to sustain a larger pressure increase than the inelastic fluids. By these arguments, and from Fig. 10, even the more dilute tylose solutions seem to have extensional viscosities above those for Newtonian fluids. In fact, Pereira and Pinho [33] also found drag reduction in turbulent fully-developed pipe flow for these tylose solutions and in spite of their small molecular weight. This is an indirect indication of an enhanced extensional viscosity, if we assume that drag reduction in turbulent pipe flows is caused by high extensional viscosities. The DNS calculations of Dimitropoulos et al. [34] and Ptasinski et al. [35], amongst others, do corroborate the fundamental link between an enhanced Trouton ratio and significant drag reduction in turbulent pipe flow.

Given the apparent relation between elastic effects and the pressure rise coefficient, and taking advantage of the approximately constant values of $C_{pb} - C_{pm}$ for a given fluid and for each flow condition, we decided to represent in Fig. 12 the average pressure rise coefficient $\overline{C_{pb} - C_{pm}}$ defined in Eq. (6) as a function of the elastic number $Re^*/We \equiv D \cdot Re^*/(U_\infty \cdot \lambda_e)$ [1]. $\overline{C_{pb} - C_{pm}}$ was calculated by numerical integration and λ_e is the relaxation time.

$$\overline{C_{pb} - C_{pm}} = \int_{Re_1}^{Re_2} (C_{pb} - C_{pm})\, dRe/(Re_2 - Re_1) \qquad (6)$$

There is a good correlation between Re^*/We and $\overline{C_{pb} - C_{pm}}$, and the same happens regardless of the definition of characteristic shear rate used to quantify the viscosity used in the Reynolds number. The differences between tylose and CMC solutions seen in Fig. 12 are probably due to the characteristic end effects of the CMC solutions (cf. reference [1]).

5. Conclusions

For Reynolds numbers below 800 a reduction of the drag coefficient with the polymer concentration was observed and the main reason for this behaviour was fluid elasticity. By reducing the turbulent shear stress in the shear layers, the entrainment of fluid by the shear layers from the formation region decreased and both the formation length [2,10] and the base pressure increased. The latter compensated the reduction in the turbulent shear stress to maintain the equilibrium of forces within the recirculating bubble, in this way reducing the drag coefficient.

The pressure rise coefficient did not change appreciably with the Reynolds number, and for the tylose solutions there was a clear increase in $C_{pb} - C_{pm}$ with polymer concentration. Globally, the effects of the critical Reynolds numbers and formation length on the pressure rise coefficient were weak.

The perturbations observed by Coelho and Pinho [2] at the edges of the cylinder with CMC solutions could be

responsible for the higher scatter of pressure related data and could also account for the differences between tylose and CMC solutions: the apparent independence of C_D on the polymer concentration for the CMC solutions in contrast to results for the tylose solutions.

Within the shear-layer transition regime, there was a reduction of l_f/l_{fc} with the polymer concentration, but this did not rise the drag coefficient, in fact quite the opposite: fluids showing the highest reduction of l_f/l_{fc} had the lowest drag coefficient. This was due to the simultaneous increase of the wake angle and the pressure rise coefficient with polymer concentration, both of which concur to reduce C_D by narrowing the wake.

Apparently, the ability of the boundary layer to sustain an higher pressure rise prior to separation, i.e. higher values of $C_{pb} - C_{pm}$, that reduce the drag coefficient by narrowing the wake, overshadows the opposite effect on C_D of transition taking place in the free shear layers.

A good correlation between the elastic number Re^*/We and the pressure rise coefficient $\overline{C_{pb} - C_{pm}}$ was found and this was fairly insensitive to the characteristic shear rate used to quantify the characteristic viscosity.

Acknowledgements

The authors wish to thank JNICT for the financial support through project PBIC/C/CEG/1370/92 and the equipment lent by INEGI and IDMEC. P.M. Coelho also wishes to thank University of Porto for the leave of teaching duties between 1993 and 1996 which made possible a significant portion of this work.

References

[1] P.M. Coelho, F.T. Pinho, Vortex shedding regimes in cylinder flow of shear-thinning fluids. I. Identification and demarcation, J. Non-Newtonian Fluid Mech. 110 (2003) 143–176.
[2] P.M. Coelho, F.T. Pinho, Vortex shedding regimes in cylinder flow of shear-thinning fluids. II. Flow characteristics, J. Non-Newtonian Fluid Mech. 110 (2003) 177–193.
[3] M.J. Shah, E.E. Petersen, A. Acrivos, Heat transfer from a cylinder to a power-law Non-Newtonian fluid, AIChE J. 8 (1962) 542–549.
[4] A. White, Drag of spheres in dilute high polymer solutions, Nature 216 (1967) 994–995.
[5] J.W. Hoyt, R.H.J. Sellin, Cylinder cross-flow heat transfer in drag-reducing fluid, Exp. Heat Transfer 2 (1989) 113–127.
[6] D.F. James, A.J. Acosta, The laminar flow of dilute polymer solutions around circular cylinders, J. Fluid Mech. 42 (1970) 269–288.
[7] D.F. James, O.P. Gupta, Drag on circular cylinders in dilute polymer solutions, Chem. Eng. Prog. Symp. Ser. 67 (1971) 62–73.
[8] T. Sarpkaya, P.G. Rainey, R.E. Kell, Flow of dilute polymer solutions about circular cylinders, J. Fluid Mech. 57 (1973) 177–208.
[9] M. Kiya, M. Arie, S. Shoda, An increase in base pressure by polymer solutions added to separated shear layers, Trans. A.S.M.E, J. Fluids Eng. 102 (1980) 376–383.
[10] O. Cadot, M. Lebey, Shear instability inhibition in a cylinder wake by local injection of a viscoelastic fluid, Phys. Fluids 11 (1999) 494–496.
[11] H. Kato, Y. Mizuno, An experimental investigation of viscoelastic flow past a circular cylinder, Bull. JSME 26 (1983) 529–536.
[12] A.B. Metzner, G. Astarita, External flow of viscoelastic materials: fluid property restrictions on the use of velocity-sensitive probes, AIChE J. 13 (1967) 550–555.
[13] E.J. Novotny Jr., R.E. Eckert, Direct measurement of hole error for viscoelastic fluids in flow between infinite parallel plates, Trans. Soc. Rheol. 17 (N°2) (1973) 227–241.
[14] K. Higashitani, A.S. Lodge, Hole pressure error measurements in pressure-generated shear flow, Trans. Soc. Rheol. 19 (N°2) (1975) 307–335.
[15] M.P. Escudier, F. Presti, S. Smith, Drag reduction in the turbulent pipe flow of polymers, J. Non-Newtonian Fluid Mech. 81 (1999) 197–213.
[16] R.B. Bird, R.C. Armstrong, O. Hassager, Dynamics of polymeric liquids, vol. 1, Fluid Mechanics, John Wiley & Sons, 1987.
[17] O. Güven, C. Farrel, V.C. Patel, Surface-roughness effects on the mean flow past circular cylinders, J. Fluid Mech. 98 (1980) 673–701.
[18] C. Farell, S. Carrasquel, O. Güven, V.C. Patel, Effect of wind-tunnel walls on the flow past circular cylinders and cooling tower models, J. Fluids Eng. 99 (1977) 470–479.
[19] D. Surry, Some effects of intense turbulence on the aerodynamics of a circular cylinder at subcritical Reynolds number, J. Fluid Mech. 52 (1972) 543–563.
[20] A. Roshko, Experiments on the flow past a circular cylinder at very high Reynolds number, J. Fluid Mech. 10 (1961) 345–356.
[21] E.C. Maskell, A theory of blockage effects on bluff bodies and stalled wings in a closed wind tunnel, R. & M. No. 3400, 1963.
[22] G.S. West, C.J. Apelt, The effects of tunnel blockage and aspect ratio on the mean flow past a circular cylinder with Reynolds number between 10^4 and 10^5, J. Fluid Mech. 114 (1982) 361–377.
[23] C. Norberg, An experimental investigation of the flow around a circular cylinder: influence of aspect ratio, J. Fluid Mech. 258 (1994) 287–316.
[24] H. Persillon, M. Braza, Physical analysis of the transition to turbulence in the wake of a circular cylinder by three-dimensional Navier–Stokes simulation, J. Fluid Mech. 365 (1998) 23–88.
[25] S. Balachandar, R. Mittal, F.M. Najjar, Properties of the mean recirculation region in the wakes of two-dimensional bluff bodies, J. Fluid Mech. 351 (1997) 167–199.
[26] A. Acharya, R.A. Mashelkar, J. Ulbrecht, Flow of inelastic and viscoelastic fluids past a sphere. I. Drag coefficient in creeping and boundary-layer flows, Rheol. Acta 15 (1976) 454–470.
[27] A. Acharya, R.A. Mashelkar, J. Ulbrecht, Flow of inelastic and viscoelastic fluids past a sphere. II. Anomalous separation in the viscoelastic fluid flow, Rheol. Acta 15 (1976) 471–478.
[28] C. Chyu, J.-C. Lin, J. Sheridan, D. Rockwell, Kármán vortex formation from a cylinder: role of phase-locked Kelvin–Helmhotz vortices, Phys. Fluids 7 (1995) 2288–2290.
[29] A. Prasad, C.H.K. Williamson, The instability of the shear layer separating from a bluff body, J. Fluid Mech. 333 (1997) 375–402.
[30] H.G.C. Woo, J.E. Cermark, J.A. Peterka, Secondary flows and vortex formation around a circular cylinder in constant-shear flow, J. Fluid Mech. 204 (1989) 523–542.
[31] J.A. Son, T.J. Hanratty, Numerical solution for the flow around a cylinder at Reynolds numbers of 40, 200 and 500, J. Fluid Mech. 35 (1969) 369–386.

[32] O. Cadot, S. Kumar, Experimental characterisation of viscoelastic effects on two- and three-dimensional shear instabilities, J. Fluid Mech. 416 (2000) 151–172.
[33] A.S. Pereira, F.T. Pinho, Turbulent pipe flow characteristics of low molecular weight polymer solutions, J. Non-Newt. Fluid Mech. 55 (1994) 321–344.
[34] C.D. Dimitropoulos, R. Sureshkumar, A.N. Beris, Direct numerical simulation of viscoelastic turbulent channel flow exhibiting drag reduction: effect of the variation of rheological parameters, J. Non-Newt. Fluid Mech. 79 (1998) 433–468.
[35] P.K. Ptasinski, B.J. Boersma, F.T.M. Nieuwstadt, M.A. Hulsen, B.H.A.A. Van den Brule, J.C.R. Hunt, Turbulent channel flow near maximum drag reduction: simulations, experiments and mechanisms, J. Fluid Mech. 490 (2003) 251–291.